*Sādhanā* (2023)48:279
https://doi.org/10.1007/s12046-023-02357-z



# Topology optimization of pelvic resection prostheses

S RAJARAMAN and SOURAV RAKSHIT*

Department of Mechanical Engineering, Indian Institute of Technology Madras, Chennai, India
e-mail: srakshit@iitm.ac.in

MS received 12 May 2023; revised 9 October 2023; accepted 11 October 2023

**Abstract.** This work proposes a new design method for pelvic prostheses based on topology optimization. Current pelvic prosthesis designs do not replicate the shape and mechanical properties of a natural pelvis as the prostheses are mostly made from metal alloys, which makes them heavier than natural pelvic bone. However, with rapid progress in additive manufacturing technologies, in the near future, it may be possible to fabricate using bio-compatible alloy topology-optimized lattice cells emulating the mechanical properties of the pelvic bone. This work proposes prosthesis designs where a significant amount of bone is resected from the hemi-pelvis, namely, type-I and combined type-II and type-III resections, which result in significant deformity of the pelvic zone, and hence for its restoration, prostheses matching the shape of resected bones are required. The prostheses are designed considering mechanical loads of walking that are exerted on the pelvic bone from muscles and the femur bone, which is new in the literature. The design is posed as a compliance minimization problem and solved using density interpolation. To reduce the stress shielding effect, the mass of prostheses is restricted to the mass of the resected bone. The densities are mapped to different types of 3-D printable lattice cells to achieve physically realizable designs. The properties of these cells are studied using compression test simulations. In summary, our proposed methodology is a prospective tool for patient-specific prostheses design.

**Keywords.** Compliance minimization; walking gait loads; topology optimization; lattice models; additive manufacturing; ANSYS®.

## 1. Introduction

The pelvis is one of the high-load-bearing skeletal structures in the human body, and the significance of pelvic girdle rehabilitation is accentuated by the high mortality rates associated with pelvic trauma [1]. Although the pelvic bone continuously adapts itself to routine activities, accidents, and tumors damage the pelvic region beyond the self-healing threshold of the bone, resulting in loss of gait stability and locomotion. Rehabilitation from tumors, in particular, necessitates orthopedic resection of bones and restoration of the pelvic region through bone grafts and prostheses. However, for pelvic resections, due to the complex shape of the hemi-pelvis, bone grafts rarely reconstruct the exact anatomy of the resected bone. This work proposes a design methodology for designing pelvic prostheses for resection of the iliac wing (type-I) and periacetabular and pubic rami zones (type-II and type-III) of the pelvic bone due to sarcoma or accidents, as shown in figure 1(a and c) respectively. Sarcoma in the pelvis requires limb salvage surgery with higher margins to prevent the recurrence of a malignant tumor. The prosthesis should preserve the shape of the pelvis to ensure fewer complications and facilitate sufficient muscle attachment areas; at the same time, it should be lightweight and provide adequate mechanical strength to restore the normal functioning of the pelvis. Existing prosthesis designs for the pelvis consist of either a reverse-engineered prosthesis (developed from scanned images of the pelvis) or a simplified beam section [2]. The former leads to longer manufacturing time and complications after surgery, while the latter is oversimplified for strength. Commercially available prostheses do not fit the anatomy of a patient precisely and lead to prosthesis loosening and associated complications. Hence, this work proposes a design methodology to design a tailor-made pelvic prosthesis similar in shape and weight to the resected part using topology optimization (TO).

Bio-compatible metals and alloys with higher elastic modulus than bone tissue are used to manufacture implants and prostheses due to their high strength and longer fatigue life. When there is a mismatch in the elastic modulus of bone and implant, the implant takes up a significant proportion of the bio-mechanical loads, called the stress shielding effect. Under such conditions, the bone cells do not have sufficient load stimulation for bone remodeling, which leads to bone resorption and, consequently, the loosening of implants, resulting in clinical complications. Moreover, the higher mass of metal prosthesis increases the

*For correspondence
Published online: 09 December 2023

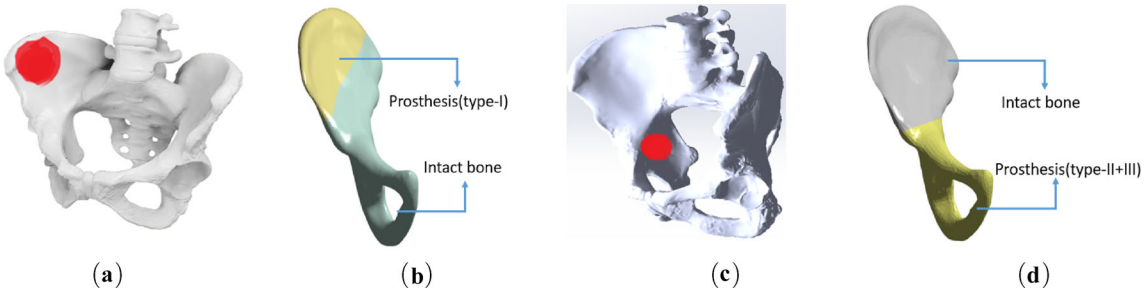


**Figure 1.** Pelvic bone with the tumor for type-I (top) and combined type-II and type-III (bottom) resections. (**a**) The red region depicts the tumor-affected zone on the iliac wing of the pelvic bone. (**b**) The colored (yellow) region shows the section where the bone is resected and substituted by the designed prosthesis. (**c**) The red region depicts the tumor-affected zone on the ischial spine region of the pelvic bone. (**d**) The colored (yellow) region shows the section where the bone is resected and substituted by the designed prosthesis.

strain on intact bone, resulting in higher muscular effort and increased energy expenditure [2]. Hence, solid metal prosthesis as proposed in Kumar and Rakshit [3] is avoided. Thus, an ideal prosthesis should have similar strength and stiffness as a natural bone and, at the same time, ensure bio-compatibility and stable fixation requirements. The stiffness and mass of prostheses can be reduced by making them porous [4–6]. However, porosity also decreases mechanical and fatigue strength. Thus, optimization-based designs aim to find the trade-off between stiffness, mechanical strength, and bio-compatibility requirements of the prosthesis. Jang and Kim [7] used micro finite element-based TO to design a 2-D bone micro-structure with significant similarities with the trabecular bone of the femur. Sutradhar *et al* [8] used TO to design craniofacial implants. Wu *et al* [9] generated infill patterns similar to the femur bone trabecular region where local volume constraints were imposed on the modified SIMP (Solid Isotropic Material with Penalization) based voxel TO formulations. With significant advances in additive manufacturing (AM), various sizes and shapes of porous lattice structures can now be 3-D printed. Two new micro-structures showing prospects for prostheses and implants are Triply Periodic Minimal Surface (TPMS) and Voronoi cell-based lattices. TPMS lattices do not require any support structure during 3-D printing and offer higher specific stiffness and strength compared to other lattices. Voronoi lattices replicate the architecture of trabecular bone [10]. Thus, a combined approach of TO-based design and its fabrication using AM may provide a prospective method for patient-specific development of prosthesis that matches the mechanical properties of resected bones and at the same time satisfies bio-compatibility requirements [5].

This work proposes an improved design methodology of patient-specific prosthesis design for type-I, II, and III pelvic resections (figure 1) using TO on our previous work in Rajaraman and Rakshit [11]. The prosthesis is designed for maximal stiffness subject to walking gait loads with a mass constraint equal to the mass of the resected bone. The material chosen is Ti–6Al–4V for its excellent bio-compatibility properties. The tailor-made material properties in the prosthesis are achieved using shell and lattice infill architecture that can be fabricated using AM. This shell and infill architecture ensures that the structure facilitates muscle attachment areas and a conformal geometry similar to the resected bone and helps in easier implant interfacing with intact bone. This architecture provides additional cosmetic benefits of no depression or cavity in the resected region. The shell part is determined based on AM manufacturability constraints for the prosthesis material. The infill part consists of different strut and TPMS lattices, the thickness of which is determined by mapping the density field solved from a weighted compliance minimization problem solved using TO. The prosthesis containing different strut and TPMS cells are then compared for stiffness using simulated compression test experiments. To the best of our knowledge, this is the first work on the TO-based design of a functionally graded pelvic prosthesis, taking into account walking gait loads and in-situ constraints like muscle attachment with bone. Further, the performance of the different types of lattice cells in the designed prostheses is explored.

The rest of the paper is organized as follows: In section 2, we first describe the design domain and material properties of the pelvic bone used in optimization and boundary conditions applied to the pelvic resection models. Section 2.3 introduces the different procedures used for designing and testing the prostheses, followed by sections describing these procedures. Section 3 presents the optimal density results from TO for type-I and combined type-II and type-III resections, stress shielding measures calculated using two different metrics for walking gait loads, and

results of the compression test simulations to judge the performance of different types of lattice units. In section 4, the paper ends with a discussion and concluding remarks.

## 2. Methods

### 2.1 *Design domain model*

The geometric model of the pelvis is purchased from the TurboSquid domain. The model is built from laser topography with a 3D laser scanner with an accuracy of 0.1 mm. The surface mesh model is converted into a 10-noded tetrahedral-based volume mesh, which is further used to create a watertight solid hemi-pelvic bone CAD model [13, 14]. The surface mesh is then corrected for self-intersections and is mirrored to match the anthropometric details mentioned in Dostal and Andrews [12]. Dalstra *et al* [15] suggested a homogeneous cortical thickness and elastic modulus for trabecular bone was appropriate for comparative studies than patient-specific modeling. Hence, A uniform thickness of 1.41 mm is assigned to the cortical shell [16]. The cortical bone is assumed homogeneous with the elastic modulus of 17 GPa, Poisson's ratio of 0.3, and material density of 1800 kg/m$^3$. Similarly, the trabecular bone is assigned material properties of elastic modulus of 0.338 GPa, Poisson's ratio of 0.2, and material density of 483 kg/m$^3$ [16].

The TO design domain comprises the volume of the resected bone as shown in figure 1(b) for type-I resection and figure 1(d) for combined type-II and type-III resections. Ti–6Al–4V alloy is chosen as the material for the prosthesis due to its excellent bio-compatibility, stiffness-to-weight ratio, mechanical strength, and ease of manufacturability. Ti–6Al–4V has an isotropic elastic modulus of 114 GPa and Poisson's ratio of 0.34. The geometric and mass parameters of the pelvic bone and solid prosthesis using Ti–6Al–4V for type-I and combined type-II and type-III resections is given in table 1. Hence, if solid Ti–6Al–4V is used, then the mass of the prosthesis will be 0.271 kg against 0.063 kg of bone for type-I resection and 0.634 kg for prosthesis against 0.126 kg of resected bone for combined type-II and type-III resections, making the prosthesis much heavier than resected bone. To preserve compatibility, the shape of the prosthesis is made the same as that of the resected bone with a uniform shell thickness of 0.4 mm as suggested for additively manufactured titanium-based structures [17]. This shell is excluded from the design domain in the TO optimization problem. Thus, the design domain of the prosthesis consists of the volume of the resected bones as shown in figures 1b and d without the uniform shell thickness of 0.4 mm.

### 2.2 *Boundary conditions*

The hemi-pelvis model is fixed at the sacro-iliac joint and pubic symphysis as shown in figure 2(a). A study made by Clarke et al. [18] suggested that a restraint on all degrees of freedom was sufficient to model sacro-iliac joint and pubic symphysis over the inclusion of ligamentous boundary conditions. Hence, the displacement degrees of freedom (DOF) in the sacro-iliac joint and pubic symphysis region are completely restrained. The musculoskeletal loading comprises forces from the set of 21 muscles (muscle attachment areas on pelvic bone shown in figure 2b) and hip joint force during the eight phases of the walking gait cycle as shown in figure 3. The magnitude of the walking gait loads are obtained from Dalstra and Huiskes [19]. The weight fractions of the multi-loads are determined based on the percentage of occurrence of a gait cycle over the entire cycle duration [19]. The weight values corresponding to the eight phases of the gait cycle starting from I to VIII (figure 3) are 0.04, 0.11, 0.22, 0.13, 0.04, 0.11, 0.22, and 0.13, respectively. The muscle attachment areas identified on the pelvic cortex are adapted from Dalstra et al. [15].

**Table 1.** Geometric and mass parameters of the pelvic bone and prosthesis for type-I resection and combined type-II and type-III resections.

| Parameter | Units | Type-I | Combined type-II and III |
|---|---|---|---|
| Iliac breadth | mm | 165 | 165 |
| Coxal height | mm | 230 | 230 |
| Volume of hemi-pelvic bone | mm$^3$ | 290,563.50 | 290,563.50 |
| Density of cortical shell | kg/m$^3$ | 1800.0 | 1,800.0 |
| Density of trabecular core | kg/m$^3$ | 483.0 | 483.0 |
| Density of Ti–6Al–4V implant | kg/m$^3$ | 4429.0 | 4429.0 |
| Mass of pelvic bone | kg | 0.261 | 0.261 |
| Volume of resected bone | mm$^3$ | 61,305.46 | 142,315.10 |
| Mass of resected bone | kg | 0.063 | 0.126 |
| Mass of solid Ti–6Al–4V implant | kg | 0.271 | 0.634 |
| Mass fraction | – | 0.232 | 0.199 |

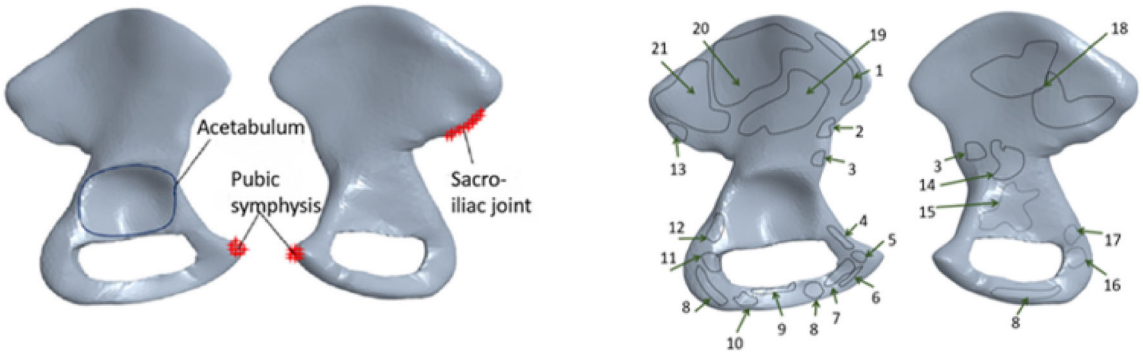


**Figure 2.** Boundary conditions on the hemi-pelvic bone. (**a**) Fully restrained DOF at the sacro-iliac joint and pubic symphysis with the reaction at the acetabulum (**b**) Representative muscle attachment areas adopted from [19, 20].

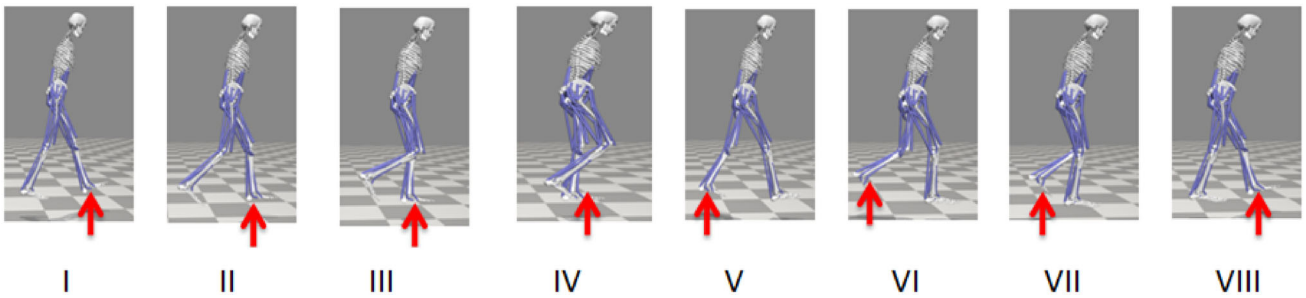


**Figure 3.** Eight phases of the walking gait cycle. The red arrow indicates the leg being tracked. The eight phases are (**I**) Double support beginning stance (**II**) Beginning single support (**III**) Halfway single support (**IV**) End single support (**V**) Double support end stance (**VI**) Beginning swing (**VII**) Halfway swing (**VIII**) End swing. The figures are created using OpenSim® software.

The muscle line of action for the finite element (FE) model is obtained by subtracting the coordinates of distal and proximal insertion regions from the work of Dostal and Andrews [12], and the hip joint force directions are adapted from the work of Bergmann et al. [21]. Although we have not encountered any technology for attaching all muscles to pelvic prostheses, we assume this technology will be developed and employed in the future. The FE model comprises the intact bone and the pelvic prosthesis. Bonded contacts are assigned to the contact elements between the cortical shell and trabecular core and between the prosthesis and the intact bone interface. This work does not consider the design of screws at the prosthesis bone interface.

## 2.3 *Prostheses design method*

Figure 4 shows a pictorial summary of the methodology for this work. After constructing the design domain and applying the boundary conditions, SIMP-based TO is used to design the density profile of prostheses. Next, this density profile is mapped onto different types of lattices using nTopology®software. Prostheses with different lattices are tested for stiffness by compression test simulation. The following subsections give a brief description of each procedure.

## 2.4 *TO for multiple load-case compliance minimization*

Topology optimization (TO) is widely used to distribute material optimally within a given design domain subjected to a set of constraints. The binary, void, or solid material distribution poses numerical instabilities to the optimization algorithm, and hence, these instabilities are circumvented using the SIMP technique. SIMP converts the binary void or solid material distribution into a continuous material distribution problem using a fictitious density variable ($\rho$). The optimization formulation penalizes this density variable to steer the continuous density variable towards solid ($\rho = 1$) or void ($\rho = 0$).

The optimization problem for the prosthesis is posed as a weighted compliance minimization problem subject to walking gait cycle loads [11]. A weighted multi-load approach is followed to consider the gait loads of all the eight phases of the walking gait cycle [22, 23] as shown in

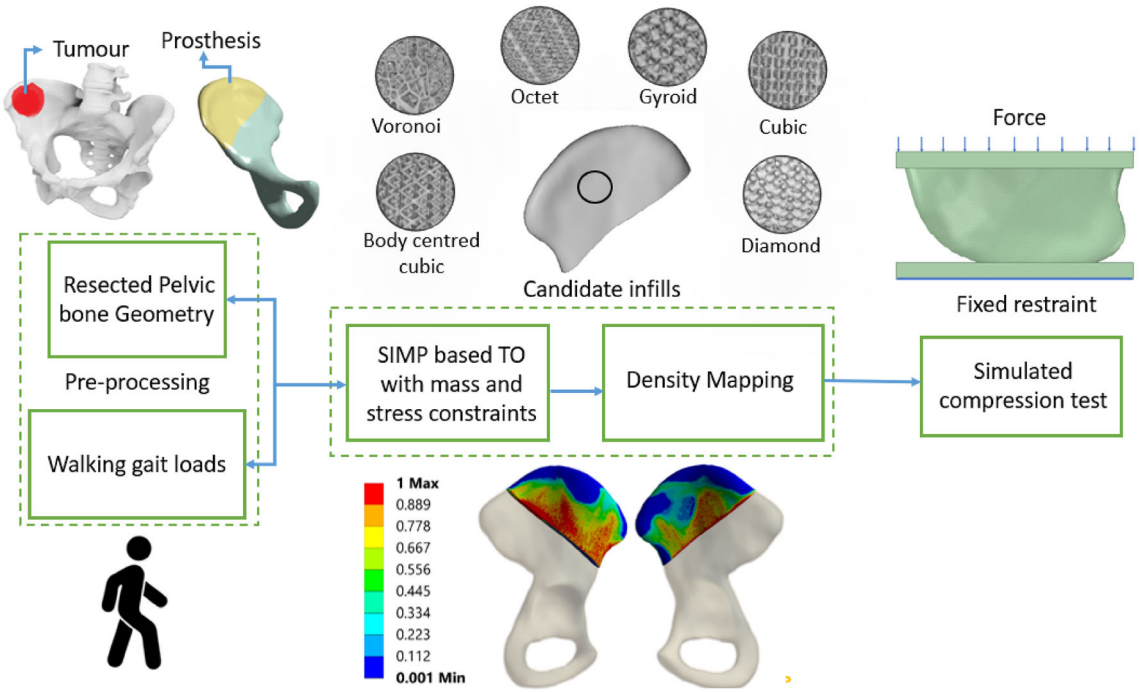


**Figure 4.** Flowchart of the methodology for the design optimization of the pelvic prosthesis. Pre-processing consists of design domain, loading and fixed boundary conditions, and material properties of prosthesis. TO is done using the SIMP model, which gives a density profile of the resected part (bottom). This density profile is mapped to different types of lattices (top). The performance of different lattices in the prosthesis is evaluated by simulation of compression test experiment.

figure 3. Mass constraints are imposed to match the exact mass of the resected bone. These constraints ensure that there are no additional strains on intact bone due to the additional mass of the prosthesis. The optimization program takes in the input design domain of solid prosthesis as shown in figure 1(b and d) and optimizes the design variable ($\rho$) to minimize the weighted compliance ($c$) and, at the same time restrict to the mass fraction mentioned in table 1. The multi-load case compliance minimization problem is posed as:

$$\begin{aligned} \min_{\rho_1,\rho_2\cdots\rho_N} \quad & C = \textstyle\sum_{i=1}^{8} w_i \mathbf{f}_i^T \mathbf{u}_i \\ \text{s.t.} \quad & \mathbf{K}\mathbf{u}_i = \mathbf{f}_i \\ & \textstyle\sum_{e=1}^{N} \rho_e m_e \le M \\ & \rho_{min} \le \rho \le \rho_{max} \\ & \sigma_e \le \sigma_{max} \\ & \mathbf{k}_e = \rho_{\mathbf{e}}{}^p \mathbf{k}_0 \end{aligned} \tag{1}$$

$\mathbf{k}_e$ and $\mathbf{k}_0$ are the modified elemental stiffness matrix and elemental stiffness matrix of solid ($\rho = 1$) Ti–6Al–4V element, respectively. $N$ is the number of finite elements of the prosthesis model. Maximum stress ($\sigma_{max}$) limit of 680 MPa [24] is imposed on the Ti–6Al–4V prosthesis to meet the requirement of 10 million cycles of the prosthesis. $\rho_{min}$ is assigned 0.001 to overcome numerical singularities and $\rho_{max}$ is assigned a maximum value of 1.

## 2.5 *Stress Constraint Implementation in TO*

Theoretically, the number of stress constraints equal to the number of finite elements (excluding non-design domains) must be imposed. However, this requires very high computational power. The solver uses a relaxed formulation instead, where clusters of elements are formed, and the maximum von Mises stress value satisfies the stress constraint. Let $\sigma_s$ denote the set of all stress values of the elements in cluster $S$. Hence, the stress constraints are formulated as

$$\max_{e \in S} \sigma_e \le \sigma_{max} \tag{2}$$

The maximum function in equation 2 is non-differentiable; hence, a $p$-norm is used to approximately represent the actual maximum elemental von Mises stress.

$$\max_{e \in S} \sigma_e = ||\sigma_s||_\infty \le ||\sigma_S||_p \tag{3}$$

Since the $p$-norm overestimates the maximum stress an adaptive factor $C_t$ is introduced in each iteration $t$ such that:

$$\lim_{t \to \infty} C_t ||\sigma_S^t||_p \le ||\sigma_s^t||_\infty \tag{4}$$

The value of $C_t$ is estimated for iterations $t \ge 1$ as

$$C_t = \alpha_t \frac{\sigma_{max}^{t-1}}{||\sigma_S^{t-1}||_p} + (1 - \alpha_t) C_{t-1} \tag{5}$$

$\alpha_t \in (0,1]$ if $C_t$ tends to oscillate, else it is set at 1 [25, 26].

## 2.6 *Density mapping*

SIMP-based TO is a versatile and computationally efficient method for optimal material distribution. Although the SIMP method is computationally efficient, the optimal results of the SIMP-based TO are not physically realizable owing to a range of densities in the optimal result. One way to physically realize the SIMP-based TO results is to map the densities of SIMP into equivalent lattice structures, which can then be manufactured using AM [27]. Also, SIMP-based TO is computationally more efficient than lattice-based homogenization used in our previous work [28]. Hence, to physically realize the density distribution of SIMP, we map the results of the SIMP density field into lattice units.

The lattice units considered for pelvic prosthesis design include strut-based and TPMS lattice units (figure 5). The strut-based lattice cells are comprised of the cubic, body-centered cubic, octet, and Voronoi-based lattices. The gyroid and diamond lattices belong to the family of TPMS lattice units. The TPMS lattice units are generally represented by level set equations that are functions of a parameter $\phi$, which controls its relative density. The level set equations of gyroid and diamond at a point with coordinates $(x, y, z)$ are defined as follows:

**Gyroid :** $\sin(x)\cos(y) + \sin(y)\cos(z) + \sin(z)\cos(x) - \phi = 0$

**Diamond :** $\sin(x)\sin(y)\sin(z) + \sin(x)\cos(y)\cos(z) + \cos(x)\sin(y)\cos(z) + \cos(x)\cos(y)\sin(z) - \phi = 0.$

The Voronoi cells are generated by random generation of seed points within the TO design domain with a constant spacing distance of seed points. These lattice units are classified under stochastic lattices. The directional elastic modulus of the lattice cells as a heat map is also shown in figure 5. The red and blue contours in the heat map correspond to the maximum and minimum elastic modulus values, respectively. The octet, gyroid, and diamond lattices show more isotropic material properties, while the cubic and body-centered cubic lattices show very high anisotropy. The octet lattice cells are stretch-dominated, while the others are bend-dominated and compliant. The density field results of the SIMP-based TO of the infill volume are mapped onto the thickness of the lattice elements using barycentric linear interpolation of the three closest nodes. The relative density value $\rho$ from the SIMP density field is mapped to the thickness $t$ of the representative strut in strut-based lattices and the thickness of the shell in TPMS lattices. The minimum thickness of strut-based lattices is 0.6 mm, and the size of the lattice units is 7 mm. These values are determined considering the shell-lattice infill structures' comparative nature and computational cost. The maximum thickness of the strut in lattices is iteratively varied till the mass of the shell and infill structure matches the target mass constraint imposed in the TO formulation. Thus, we generate functionally graded lattices of varying lattice thicknesses using the density mapping strategy.

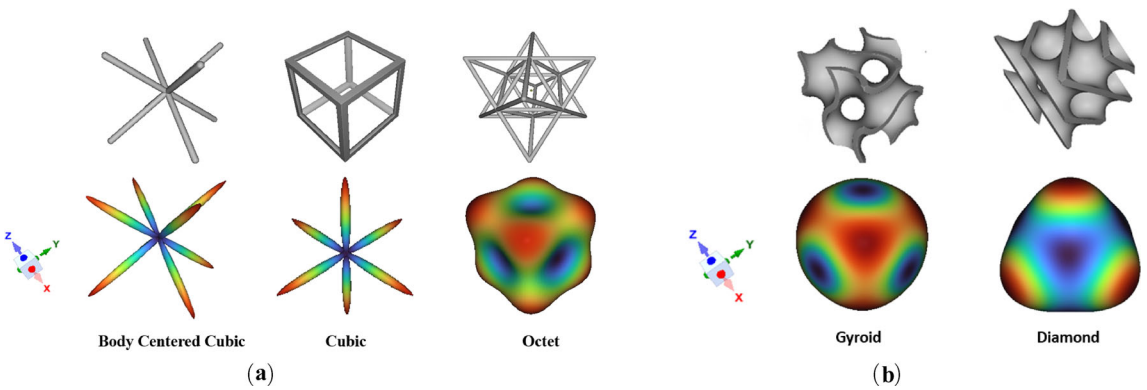


**Figure 5.** Homogenized strut and TPMS-based lattices: The top row shows the geometries. The heat map on the bottom row shows the directional elastic modulus along the three coordinate axes, with red and blue contours representing maximum and minimum trends, respectively. (**a**) Strut-based lattices: Body-centered cubic, cubic, and octet lattices. (phases of the walking gait cycle) TPMS-based lattices: Gyroid and diamond lattice.

### 2.7 *Stress shielding measurement*

One of the main goals of prosthesis design is that it should not lead to stress shielding. Stress shielding occurs when an implanted prosthesis much stiffer than natural bone deprives the resected bone of its natural state of stress, leading to bone resorption around the implanted region. In this work, two measures of stress shielding are used. The first is "Stress Shielding Signal"(*SSS*) defined by Weinans *et al* [29]:

$$SSS = \frac{SE(\text{bone+implant}) - SE(\text{intact bone})}{SE(\text{intact bone})} \tag{6}$$

where *SE* is the strain energy or compliance of the intact bone or bone with the implant.

The second measure of stress shielding that we have used is "Stress Shielding Increase" (*SSI*) defined by Fraldi *et al* [30]:

$$SSI = \frac{\langle \sigma_{VMS}^{\text{intact}} \rangle - \langle \sigma_{VMS}^{\text{bone+implant}} \rangle}{\langle \sigma_{VMS}^{\text{intact}} \rangle}$$
$$\text{where} \quad \langle \sigma_{VMS}^{\text{intact}} \rangle = \frac{1}{\sum_e V^e} \int_{V^e} (\sigma_{VMS}^{\text{intact}})^e dV \quad \text{and} \tag{7}$$
$$\langle \sigma_{VMS}^{\text{bone+implant}} \rangle = \frac{1}{\sum_e V^e} \int_{V^e} (\sigma_{VMS}^{\text{bone+implant}})^e dV$$

are the averages of von Mises stresses over the selected volume elements *e*. For this work, the 'intact' bone is the hemi-pelvic bone.

### 2.8 *Compression test simulation*

The material of prostheses is tested for strength using compression tests [31, 32]. Following this procedure, we have simulated compression tests on the lattice-infilled prostheses using ANSYS® software. In the compression test, one end of the prosthesis is fixed to a stationary support, and on the other end, a continuous force is applied using the loading plate. The boundary conditions for compression test simulation are shown in figure 6, which is similar to the compression test done for bones [15]. All degrees of freedom are restrained on nodes on the fixed restraint end, and on the other end, a uniformly distributed force equal to three times the body weight (maximum load acting on the pelvic bone [21]) is applied as shown in figure 6. The ratio of applied load to the maximum displacement gives a sense of stiffness of the prosthesis.

### 2.9 *Topology optimization (TO) solver*

We use ANSYS® Academic Research Mechanical, Release 2020 R1 topology optimization module to solve the SIMP-based multiple load-case weighted compliance minimization TO problem as formulated in equation 1. 10-noded

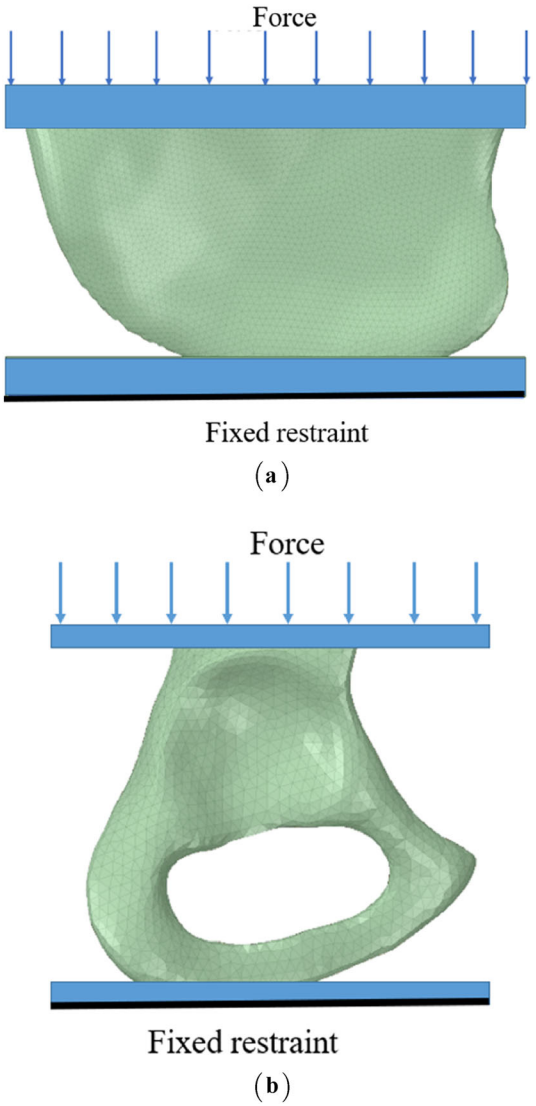


**Figure 6.** Boundary conditions for the compression simulations (**a**) Type-I resection prosthesis (**b**) Type-II+III resection prosthesis.

tetrahedral elements are used for the FE mesh, which consists of 25107 elements for type-I prosthesis and 27175 elements for combined type-II and type-III prosthesis (figure 1b and d). An average mesh size of 4 mm was used after a mesh convergence study. The simulations were performed on a computer with 32 GB of RAM and Intel® Core i5, 3.60 GHz processor. The simulations take approximately 7.5 and 24 hours to optimize prosthesis for type-I and combined type-II and type-III resections, respectively. The optimization program uses sequential convex programming in addition to the method of moving asymptotes (MMA) [33] for faster convergence [34]. Convergence is set to be achieved when the difference between the objective (weighted compliance) values of subsequent iterations is not more than 1 %. This value of convergence tolerance ensures a tight convergence limit

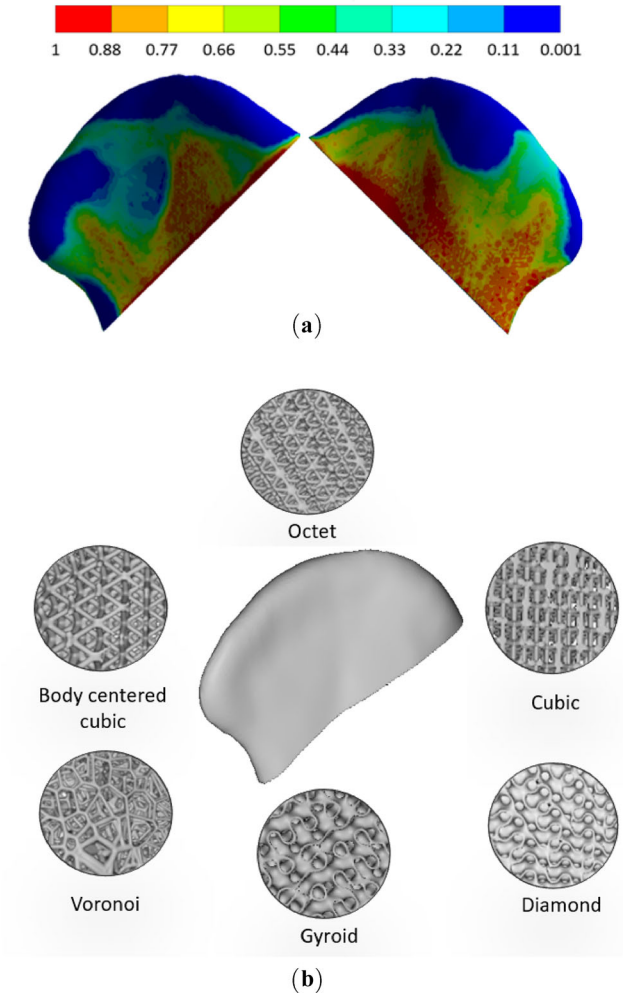


**Figure 7.** (**a**) Relative density distribution from SIMP-based topology optimization for a type-I pelvic prosthesis. The legend shows the color map of density distribution, with red representing the highest density and blue the lowest density. (**b**) Prosthesis with candidate lattice units.

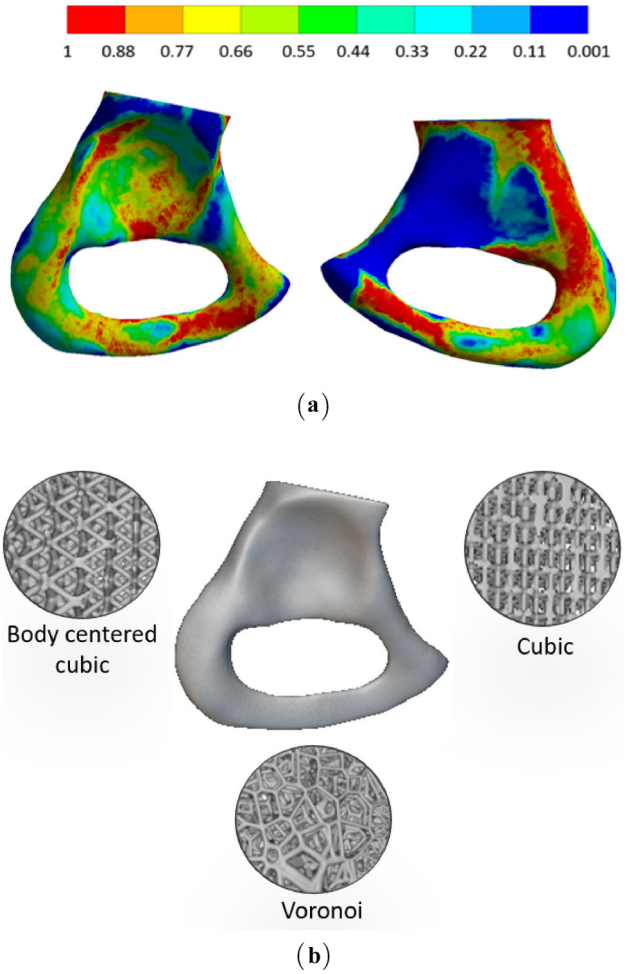


**Figure 8.** (**a**) Relative density distribution from SIMP-based topology optimization for combined type-II and type-III pelvic prosthesis. The legend shows the color map of density distribution, with red representing the highest density and blue the lowest density. (**b**) Prosthesis with candidate lattice units.

and helps the optimization algorithm avoid spurious local minimum solutions. The post-processing and the subsequent shell and lattice model generation with the simulated compression test is carried out in the nTopology® software.

## 3. Results

The optimal density field of the SIMP-based TO, along with density-mapped lattices, are shown in figures 7 and 8. The density field shows that the muscle forces significantly affect the material distribution in the prosthesis, and their inclusion in the optimization model of the prosthesis is essential. Since this work considers the effect of muscle forces in the design optimization of the prosthesis, our designs might have better functional outcomes with lesser chances of complications and implant rejections [35].

Tables 2 and 3 show the SSS measure of stress shielding (equation (6)) for type-I and combined type-II and type-III prostheses for all eight phases of gait cycle loads. The average percentage SSS for type-I solid prosthesis is 23.77%, whereas, for the density-optimized type-I prosthesis, it is around 12.80% (table 2). For combined type-II and type-III prosthesis, the average percentage SSS is 55.47% for solid prosthesis and 46.39% for the density-optimized prosthesis (table 3). When SSI is used for evaluating stress shielding, for type-I solid prosthesis, the average percentage SSI is 24.25%, whereas, for the density optimized type-I prosthesis, it is 14.04% (table 4). For combined type-II and type-III prosthesis, the average percentage SSI is 37.23% for solid prosthesis and 10.41% for the density-optimized prosthesis (table 5). Thus, for both prosthesis types, there is a marked decrease in stress shielding from switching over from solid prosthesis to density-optimized prosthesis. Further, a solid Ti–6Al–4V

**Table 2.** Stress shielding signal (SSS) in percentage calculated using equation (6) for solid and density optimized type-I pelvic prosthesis for loads from eight phases of walking gait.

| Gait phase | Pelvic bone SE (mJ) | Type-I solid implant SE (mJ) | SSS (%) for solid prosthesis relative to pelvic bone | Type-I optimized implant SE (mJ) | SSS (%) optimized prosthesis relative to pelvic bone |
|---|---|---|---|---|---|
| I | 103.98 | 97.53 | 6.20 | 112.96 | −8.64 |
| II | 101.72 | 80.71 | 20.66 | 89.77 | 11.75 |
| III | 115.35 | 83.74 | 27.40 | 105.65 | 8.41 |
| IV | 142.01 | 111.77 | 21.29 | 138.13 | 2.74 |
| V | 363.63 | 223.98 | 38.41 | 262.40 | 27.84 |
| VI | 964.29 | 493.81 | 48.79 | 556.40 | 42.30 |
| VII | 45.64 | 31.80 | 30.34 | 34.10 | 25.29 |
| VIII | 98.96 | 101.87 | −2.94 | 106.22 | −7.33 |

**Table 3.** Stress shielding signal (SSS) in a percentage calculated using equation (6) for solid and density optimized combined type-II and III pelvic prosthesis for loads from eight phases of walking gait.

| Gait phase | Pelvic bone SE (mJ) | Type-II+III solid implant SE (mJ) | SSS (%) for solid prosthesis relative to pelvic bone | Type-II+III optimized implant SE (mJ) | SSS (%) optimized prosthesis relative to pelvic bone |
|---|---|---|---|---|---|
| I | 103.98 | 62.43 | 39.96 | 72.12 | 30.64 |
| II | 101.72 | 39.65 | 61.03 | 53.44 | 47.46 |
| III | 115.35 | 59.16 | 48.73 | 73.53 | 36.25 |
| IV | 142.01 | 50.81 | 64.22 | 54.19 | 61.84 |
| V | 363.63 | 93.74 | 74.22 | 101.96 | 71.96 |
| VI | 964.29 | 237.58 | 75.36 | 279.81 | 70.98 |
| VII | 45.64 | 27.14 | 40.54 | 35.85 | 21.45 |
| VIII | 98.96 | 59.62 | 39.75 | 68.79 | 30.49 |

**Table 4.** Stress shielding increase (SSI) in percentage calculated using equation (7) for solid and density optimized type-I pelvic prosthesis for loads from eight phases of walking gait.

| Gait phase | Pelvic bone mean stress (MPa) | Type-I solid implant mean stress (MPa) | SSI (%) for solid prosthesis relative to pelvic bone | Type-I optimized implant mean stress (MPa) | SSI (%) optimized prosthesis relative to pelvic bone |
|---|---|---|---|---|---|
| I | 2.18 | 1.75 | 19.57 | 2.14 | 1.69 |
| II | 2.32 | 1.80 | 22.33 | 1.96 | 15.67 |
| III | 2.33 | 1.83 | 21.33 | 2.04 | 12.31 |
| IV | 2.68 | 2.15 | 19.83 | 2.38 | 11.07 |
| V | 4.58 | 3.20 | 30.07 | 3.57 | 21.92 |
| VI | 7.25 | 4.83 | 33.40 | 5.29 | 27.12 |
| VII | 1.58 | 1.18 | 25.16 | 1.29 | 18.16 |
| VIII | 2.30 | 1.79 | 22.31 | 2.20 | 4.38 |

prosthesis will be considerably heavier than the bone that it replaces. Another point to observe is that in a few cases, the stress shielding measure is negative (both SSS and SSI), indicating that intact bone is less stressed than bone with prosthesis. This may be due to the particular objective function used in our TO problem, namely, compliance minimization, which yields stiff prostheses, implying that average stress in designed prostheses will be reduced; hence, in the resected bone, the stress due to external load might increase as the total load on the bone remains same.

As shown in figures 7 and 8, the optimal density distribution from SIMP-based TO is mapped onto different lattice structures. The candidate lattice infills for the type-I and combined type-II and type-III prosthesis are shown in

**Table 5.** Stress shielding increase (SSI) in percentage calculated using equation (7) for solid and density optimized combined type-II and III pelvic prostheses for loads from eight phases of walking gait.

| Gait phase | Pelvic bone mean stress (MPa) | Type-II solid implant mean stress (MPa) | SSI (%) for solid prosthesis relative to pelvic bone | Type-II+III optimized implant mean stress (MPa) | SSI (%) optimized prosthesis relative to pelvic bone |
|---|---|---|---|---|---|
| I | 2.18 | 2.09 | 4.22 | 2.84 | -30.27 |
| II | 2.32 | 1.37 | 41.05 | 2.00 | 13.67 |
| III | 2.33 | 1.56 | 33.27 | 2.29 | 1.76 |
| IV | 2.68 | 1.49 | 44.43 | 2.08 | 22.24 |
| V | 4.58 | 2.07 | 54.78 | 2.87 | 37.33 |
| VI | 7.25 | 3.18 | 56.13 | 4.48 | 38.18 |
| VII | 1.58 | 1.09 | 31.17 | 1.64 | -3.67 |
| VIII | 2.30 | 1.55 | 32.82 | 2.21 | 4.0 |

figures 7(b) and 8(b), respectively. As mentioned in section 2.8, the mechanical properties of the prostheses should be evaluated before designed prostheses are put inside the human body. Following compression testing methods similar to Dalstra et al. [15], the stiffness of type-I and combined type-II and III prostheses with different lattice infills is tested through a simulated compression testing in ANSYS® software. The nodes of the iliac crest part of the prosthesis are fixed to the bottom plate for a type-I prosthesis as shown in figure 6(a). For the combined type-II and type-III prosthesis, the nodes of the ischial tuberosity part of the pelvic bone are restricted for all degrees of freedom, as shown in figure 6(b). A uniformly distributed compressive force equal to three times the body weight (maximum load acting on the pelvic bone [21]) is applied at the face of the loading plate shown in figure 6.

The results of the compression test simulation are shown in tables 6 and 7. The stiffness is inversely proportional to the displacement for a fixed load in the compression test. Table 6 shows simulated compression test results for type-I resection in which all types of lattice cells (figure 5) have been considered. The results show that the diamond lattice structure offers the highest stiffness (lowest displacement), followed by gyroid and octet. Bend-dominated TPMS lattice members, such as the gyroid and diamond lattices, provide higher stiffness per unit weight more efficiently than the stretch-dominated strut-based cubic, body-centered cubic, and Voronoi lattice cells. Although TPMS cells are stiffer than strut cells and are conducive to additive manufacturing, in particular prostheses types concerned in this work, they are not suitable as they have higher stiffness than natural bone, which may lead to stress shielding effect and consequent resorption of bone around prosthesis attachment area with bone. Further, we encountered considerable numerical difficulties with mesh connectivity for the combined type-II and type-III prosthesis for the TPMS lattices. Hence, they are excluded in the simulated compression test results in table 7 for combined type-II and type-III prosthesis. We also note from tables 6 and 7 that the peak stresses never cross 300 MPa, whereas the maximum allowed stress limit is 680 MPa. This is because of the AM fabrication constraints, which require a minimum threshold wall and strut thickness.

**Table 6.** Compression test simulation results with different lattice cells for type-I resection.

| Lattice | Maximum displacement (mm) | Maximum von Mises stress (MPa) |
|---|---|---|
| Cubic | 0.441 | 182.91 |
| Octet | 0.389 | 138.23 |
| Body centered cubic | 0.414 | 166.40 |
| Voronoi | 0.401 | 157.30 |
| Gyroid | 0.361 | 128.86 |
| Diamond | 0.332 | 132.49 |

**Table 7.** Compression test simulation results with different strut-based lattice cells for combined type-II and type-III resections.

| Lattice | Maximum displacement (mm) | Maximum von Mises stress (MPa) |
|---|---|---|
| Cubic | 0.206 | 294.12 |
| Body centered cubic | 0.205 | 252.69 |
| Voronoi | 0.215 | 262.88 |

## 4. Discussion and conclusions

This work developed a methodology to design pelvic resection type-I and combined type-II and type-III prostheses that have the same geometry as the resected bone and, at the same time, reduce the stress shielding effect that may develop in case solid metal alloy prostheses are used. For significant resections, there is a geometrical deformity

of the body around the pelvis if the prosthesis is much different in shape from that of the resected bone. Further, a prosthesis with a simple geometrical shape like a beam or cap will not provide any muscle attachment areas for the many muscles attached to the pelvic bone. This will affect the rehabilitation of the patient in his/her Activities of Daily Living (ADL), as walking is one important ADL. We designed pelvic prostheses considering the gait cycle loads, which have never been done before. Since the prostheses are geometrically exactly similar to the resected part, the muscles attached to the resected bone can be attached to the prosthesis using appropriate technology. To simultaneously make the prosthesis geometrically similar to the resected part and at the same time make it lightweight, the densities were mapped into lattice cells where the thickness of the strut or shells was directly proportional to the density variable in TO. Care was taken by iteratively varying the size of lattices and the thickness of the members so that the prosthesis could be fabricated using AM.

Our use of TO as a design tool is also comparatively new in the domain of prostheses design [36]. We used weighted compliance minimization with mass constraints to formulate the optimization problem. Another option was to minimize the mass with constraints on the compliance of the prostheses; however, in that case, the optimal density profile is such that it leads to strut and shell thickness of lattices that are not realizable using AM. We studied a variety of strut-based and TPMS lattices. From the simulated compression test results, our conclusion was that strut-based lattices like the cubic would be more suitable for reducing the stress shielding effect in the prostheses. However, this conclusion is based on the constraint on the size of the strut in the lattices. If technology is available for 3-D printing of Ti–6Al–4V for smaller lattices with a lower thickness of the shell, then other lattice types, for example, TPMS cells, might have been better candidates for optimal prostheses. Thus, the choice of lattice type is very much dependent on 3-D printing technology, with advancements in AM technologies, patient-specific prostheses designed based on optimization principles as the one proposed in this work will become a state-of-the-art method in the respective field.

## List of symbols

| | |
|---|---|
| $\rho$ | Relative density (design variable) |
| $\rho_{min}$ | Lower bound of design variable $\rho$ |
| $\rho_{max}$ | Upper bound of design variable $\rho$ |
| $w$ | Weight of load-case |
| $\mathbf{K}$ | Global stiffness matrix |
| $\mathbf{u}$ | Displacement vector |
| $\mathbf{f}$ | Force vector |
| $C$ | Compliance |
| $M$ | Mass of resected part of the pelvic bone |
| $m_e$ | Mass of a unit finite element cell |
| $N$ | Number of finite element cells in the design domain |
| $\sigma$ | Von Mises stress |
| $\sigma_{max}$ | Maximum allowable von Mises stress |
| $C_t$ | Adaptive stress factor |
| $\mathbf{k}_e$ | Finite element stiffness matrix |
| $\mathbf{k}_0$ | Finite element stiffness matrix for $\rho = 1$ |
| TO | Topology optimization |
| AM | Additive manufacturing |
| SIMP | Solid isotropic material with penalization |
| TPMS | Triply periodic minimal surface |
| WC | Weighted compliance |
| ADL | Activities of daily living |

## Acknowledgements

The authors would also like to thank the nTopology® team for providing a free license to access their software.

### Declarations

**Conflict of interest** The authors declare that there is no conflict of interest.

## References

[1] Zaharie D T and Phillips A 2018 Pelvic construct prediction of trabecular and cortical bone structural architecture. *J. Biomech. Eng.* 140(9): 091001(1–11)

[2] Iqbal T, Wang L, Li D, Dong E, Fan H, Fu J and Hu C 2019 A general multi-objective topology optimization methodology developed for customized design of pelvic prostheses. *Med. Eng. Phys.* 69: 8–16

[3] Kumar K E S and Rakshit S 2021 Design of pelvic prosthesis using topology optimization for loads in running gait cycle. *J. Inst. Eng. (India) Ser. C* 102(5): 1119–1128

[4] Wang Y, Arabnejad S, Tanzer M and Pasini D 2018 Hip implant design with three-dimensional porous architecture of optimized graded density. *J. Mech. Des.* 140(11): 111406

[5] Moussa A, Rahman S, Xu M, Tanzer M and Pasini D 2020 Topology optimization of 3D-printed structurally porous cage for acetabular reinforcement in total hip arthroplasty. *J. Mech. Behav. Biomed. Mater.* 105: 103705

[6] Rahimizadeh A, Nourmohammadi Z, Arabnejad S, Tanzer M and Pasini D 2018 Porous architected biomaterial for a tibial-knee implant with minimum bone resorption and bone-implant interface micromotion. *J. Mech. Behav. Biomed. Mater.* 78: 465–479

[7] Jang I G and Kim I Y 2008 Computational study of Wolff's law with trabecular architecture in the human proximal femur using topology optimization. *J. Biomech.* 41(11): 2353–2361

[8] Sutradhar A, Paulino G H, Miller M J and Nguyen T H 2010 Topological optimization for designing patient-specific large craniofacial segmental bone replacements. *PNAS* 107(30): 13222–13227

[9] Wu J, Aage N, Westermann R and Sigmund O 2017 Infill optimization for additive manufacturing–approaching bone-like porous structures. *IEEE Trans. Visual Comput. Graph.* 24(2): 1127–1140

[10] Wang G, Shen L, Zhao J, Liang H, Xie D, Tian Z and Wang C 2018 Design and compressive behavior of controllable irregular porous scaffolds: based on voronoi-tessellation and for additive manufacturing. *ACS Biomater. Sci. Eng.* 4(2): 719–727

[11] Rajaraman S and Rakshit S 2022 Design optimization of pelvic prosthesis for type-1 resection. In: *Proceedings of the ASME 2022 International Design Engineering Technical Conferences and Computers and Information in Engineering Conference. Volume 3A: 48th Design Automation Conference (DAC)*. V03AT03A006

[12] Dostal W F and Andrews J G 1981 A three dimensional biomechanical model of hip musculature. *J. Biomech.* 14(11): 803–812

[13] Kumar K E S and Rakshit S 2020 Topology optimization of the hip bone for gait cycle. *Struct. Multidiscip. Optim.* 62(4): 2035–2049

[14] Kumar K E S and Rakshit S 2022 Optimization based synthesis of pelvic structure for loads in running gait cycle. *Sadhana* 47(118): 47–118

[15] Dalstra M, Huiskes R and van Erning L 1995 Development and validation of a three-dimensional finite element model of the pelvic bone. *J. Biomech. Eng.* 117(3): 272–278

[16] Anderson A E, Peters C L, Tuttle B D and Weiss J A 2005 Subject-specific finite element model of the pelvis: development, validation and sensitivity studies. *J. Biomech. Eng.* 127(3): 364–373

[17] Wu Z, Narra S P and Rollett A 2020 Exploring the fabrication limits of thin-wall structures in a laser powder bed fusion process. *Int. J. Adv. Manuf. Technol.* 110(1): 191–207

[18] Clarke S G, Phillips A T M and Bull A M J 2013 Evaluating a suitable level of model complexity for finite element analysis of the intact acetabulum. *Comput. Methods Biomech. Biomed. Engin.* 16(7): 717–724

[19] Dalstra M and Huiskes R 1995 Load transfer across the pelvic bone. *J. Biomech.* 28(6): 715–724

[20] Kumar K E S and Rakshit Sourav 2020 topology optimization of the hip bone for walking using multi-load approach. In: *ASME International Mechanical Engineering Congress and Exposition, volume 84607*. V012T12A013

[21] Bergmann G, Deuretzbacher G, Heller M, Graichen F, Rohlmann A, Strauss J and Duda G N 2001 Hip contact forces and gait patterns from routine activities. *J. Biomech.* 34(7): 859–871

[22] Geraldes D M, Modenese L and Phillips A T M 2016 Consideration of multiple load cases is critical in modelling orthotropic bone adaptation in the femur. *Biomech. Model. Mechanobiol.* 15(5): 1029–1042

[23] Fernandes P, Rodrigues H and Jacobs C 1999 A model of bone adaptation using a global optimisation criterion based on the trajectorial theory of Wolff. *Comput. Methods Biomech. Biomed. Engin.* 2(2): 125–138

[24] Liu Y J, Ouyang Q L, Tian R H and Wang Q Y 2009 Fatigue properties of Ti–6Al–4V subjected to simulated body fluid. *Struct. Longevity* n2(3): 169–175

[25] Chau L, Norato J, Bruns T, Ha C and Tortorelli D 2010 Stress-based topology optimization for continua. *Struct. Multidiscip. Optim.* 41(4): 605–620

[26] Holmberg E, Torstenfelt B and Klarbring A 2013 Stress constrained topology optimization. *Struct. Multidiscip. Optim.* 48(1): 33–47

[27] Mahmoud A, Seung-Kyum C and Rosen D W 2015 Design of truss-like cellular structures using relative density mapping method. *Mater. Des.* 85: 349–360

[28] Rajaraman S and Rakshit S 2023 Multiscale Topology Optimization of Pelvic Bone for Combined Walking and Running Gait Cycles. *Comput. Methods Biomech. Biomech. Eng.* 1–17

[29] Weinans H, Sumner D R, Igloria R and Natarajan R N 2000 Sensitivity of periprosthetic stress-shielding to load and the bone-density modulus relationship in subject specific finite element models. *J. Biomech.* 33(7): 389–402

[30] Fraldi M, Esposito L, Perrella G, Cutolo A and Cowin S C 2010 Topological optimization in hip prosthesis design. *Biomech. Model. Mechanobiol.* 9(4): 389–402

[31] Bogdan L, Nes C S, Duncan D and Patrascu J M 2015 Experimental compression tests on orthopedic bone cement used in total hip replacement. *Mater. Plast.* 52(1): 125–128

[32] Corona-Castuera J, Rodriguez-Delgado D, Henao J, Castro-Sandoval J C and Poblano-Salas C A 2021 Design and fabrication of a customized partial hip prosthesis employing CT-scan data and lattice porous structures. *ACS Omega* 6: 6902–6913

[33] Svanberg K 1987 The method of moving asymptotes–a new method for structural optimization. *Int. J. Numer. Meth. Eng.* 24(2): 359–373

[34] Christian Z 2001 Global convergence of a nonlinear programming method using convex approximations. *Numer. Algorithms* 27(3): 265–289

[35] Wei S, Jian L, Quan L, Guodong L and Zhengdong C 2011 Clinical effectiveness of hemipelvic reconstruction using computer-aided custom-made prostheses after resection of malignant pelvic tumors. *J. Arthroplasty* 26(8): 1508–1513

[36] Wang X, Xu S, Zhou W, Leary M, Choong P, Quian M, Brandt M and Xie Y M 2016 1. Topological design and additive manufacturing of porous metals for bone scaffolds and orthopaedic implants: a review. *Biomaterials* 83: 127–141